# Characterization of the retinal pigment epithelium in Friedreich ataxia

Duncan E. Crombie [a], Nicole Van Bergen [a], Kathryn C. Davidson [a],
Sara Anjomani Virmouni [b], Penny A. Mckelvie [c], Vicki Chrysostomou [a], Alison Conquest [a],
Louise A. Corben [d,e], Mark A. Pook [b], Tejal Kulkarni [a], Ian A. Trounce [a], Martin F. Pera [f],
Martin B. Delatycki [d,e,g], Alice Pébay [a,*]

[a] Centre for Eye Research Australia, Royal Victorian Eye and Ear Hospital & Department of Surgery, The University of Melbourne, East Melbourne, Australia
[b] Division of Biosciences, Department of Life Sciences, College of Health & Life Sciences & Synthetic Biology Theme, Institute of Environment, Health & Societies, Brunel University London, Uxbridge, UK
[c] St. Vincents Hospital, Fitzroy , Australia
[d] Bruce Lefroy Centre for Genetic Health Research, Murdoch Childrens Research Institute, Parkville Victoria, Australia; Department of Paediatrics, The University of Melbourne, Australia
[e] School of Psychological Sciences , Monash University, Clayton, Australia
[f] Department of Anatomy and Neurosciences, The University of Melbourne, Florey Neuroscience and Mental Health Institute, Walter and Eliza Hall Institute of Medical Research, Melbourne, Australia
[g] Clinical Genetics, Austin Health, Heidelberg, Australia

## ARTICLE INFO

## ABSTRACT

We assessed structural elements of the retina in individuals with Friedreich ataxia (FRDA) and in mouse models of FRDA, as well as functions of the retinal pigment epithelium (RPE) in FRDA using induced pluripotent stem cells (iPSCs). We analyzed the retina of the FRDA mouse models YG22R and YG8R containing a human FRATAXIN (FXN) transgene by histology. We complemented this work with post-mortem evaluation of eyes from FRDA patients. Finally, we derived RPE cells from patient FRDA-iPSCs to assess oxidative phosphorylation (OXPHOS) and phagocytosis. We showed that whilst the YG22R and YG8R mouse models display elements of retinal degeneration, they do not recapitulate the loss of retinal ganglion cells (RGCs) found in the human disease. Further, RPE cells differentiated from human FRDA-iPSCs showed normal OXPHOS and we did not observe functional impairment of the RPE in Humans.

## 1. Introduction

Friedreich ataxia (FRDA) is a hereditary degenerative disease that presents with both neuronal and non-neuronal manifestations including ataxia, dysarthria, cardiomyopathy, diabetes mellitus, and impairment of auditory and visual functions [1]. Cardiomyopathy is the leading cause of death in FRDA and usually presents as a hypertrophy, which can commonly progress to dilated cardiomyopathy and arrhythmias [1]. The defective gene FRATAXIN (FXN) has been identified in the majority of affected individuals, as containing an unstable GAA repeat mutation within the first intron [2]. FXN is a nuclear-encoded mitochondrial protein involved in iron–sulfur cluster assembly, heme synthesis, and intracellular iron homeostasis [1]. The levels of FXN are reduced in individuals with FRDA, as a consequence of its reduced transcription due to interference caused by the expanded GAA repeats [1].

In FRDA, ophthalmic manifestations including optic neuropathy and retinitis pigmentosa-like syndrome have been described in some patients, suggesting that retinal ganglion cells (RGCs), photoreceptors and the retinal pigment epithelium (RPE) may be affected [3–5]. Most data have implicated degeneration of the optic nerve [5–8] but very little is known of the RPE layer. The RPE plays a major role in the health of the retina. Photoreceptor death can be associated with RPE impairment, as this layer plays a supportive role to the photoreceptors. Further, the RPE accumulates iron, which increases with aging and has been implicated in retinal degeneration [9–11] and linked to impairment of RPE functions such as phagocytosis [12]. Given the central role of iron in the pathogenesis of FRDA, we questioned if the RPE could also be an affected tissue in FRDA.

The difficulty in obtaining human tissue and the paucity of functional assays specific to RPE function renders the study of the RPE layer in Humans challenging. A potential way to study RPE

* Correspondance to: Centre for Eye Research Australia. 1/32 Gisborne Street, East Melbourne, VIC 3002, Australia. Fax: +61 3 9662 3859.
E-mail address: apebay@unimelb.edu.au (A. Pébay).

cells *in vitro* is through the differentiation of human induced pluripotent stem cells (iPSCs). iPSCs have previously been derived from individuals with FRDA [13–16], showing that the iPSCs model intergenerational repeat expansion/contraction [14], and suggesting mitochondrial abnormalities in the iPSC-derived-cardiomyocytes [13,16]. We previously reported the generation of two FRDA-iPSC lines, FA3 and FA4, which were respectively derived from individuals with 527/1058 and 751/1027 GAA repeats and showed instability in repeat numbers in culture [15]. So far, there has been no study of RPE cells from FRDA-iPSCs.

Another way to determine whether the RPE is involved in FRDA is by using animal models of the disease. The double mutant *Fxn^{tm1Mkn}*Tg(FXN)YG22Pook/J mice (YG22R), which carry a *Fxn* knock-out and a human *FXN* transgene, exhibit progressive retinal degeneration but the pathophysiology of this abnormality has not been fully characterised (https://www.jax.org/strain/010963). Using these mice and comparing them to other double mutants and controls could provide information on the pathophysiology of retinal degeneration in FRDA. In this study, we used the YG22R mice, the *Fxn^{tm1Mkn}*Tg(FXN)YG8Pook/J (YG8R) and the *Fxn^{tm1Mkn}* Tg(FXN)Y47Pook/J (Y47R) mice. The YG8R and the YG22R are homozygous for the Fxnt^{m1Mkn} (*Fxn*) targeted allele and hemizygous for the human *FXN* transgene, each with a pure GAA expansion in the first intron [17–20]. These mice differ in the GAA expansion repeats, with the YG22R having 190 GAA repeats and the YG8R having 90 and 190 GAA repeats. The Y47R control mice contain a normal GAA repeat length (9 repeats). A recent analysis of the YG22R, YG8R and Y47R mice show reduced levels of human FXN protein to 60% in the YG22R and to 76% in the YG8R in comparison to the levels observed in the control Y47R in the brain with some gender variability [21]. Little is known on the impact the genetic mutations in these models have on the RPE.

Here we used three approaches: mouse models, human post mortem eyes and iPSC-derived RPE cells-to gain a better picture on the health of the RPE in FRDA and to determine if any obvious defects could be modeled *in vitro*.

## 2. Material and methods

### 2.1. Ethics

All experimental work performed in this study was approved by the Human Research Ethics committees of the Eye and Ear Hospital (09/921H, 11/1031H, 12/1091H) and the University of Melbourne (0605017, 0829937) and the UK Home Office animal licence PPL30/3031, and completed in accordance with the requirements of the National Health & Medical Research Council of Australia and the Declaration of Helsinki. This research also adheres to the ARVO statement for the use of animals in ophthalmic and vision research. For retrieval of human tissue, autopsies and eye removal were performed after a legally responsible family member gave formal permission. The Institutional Review Board of Veterans Affairs Medical Center in Albany, New York, USA, approved the collection of the autopsy samples for research, their processing and distribution to researchers, and the posthumous collection of clinical data.

### 2.2. Mouse tissue collection and processing

The following mouse models of FRDA were used: *Fxn^{tm1Mkn}*Tg(*FXN*)YG8Pook/J mouse (YG8R), the *Fxn^{tm1Mkn}* Tg(*FXN*)YG22Pook/J mouse (YG22R) and the *Fxn^{tm1Mkn}* Tg(FXN)Y47Pook/J (Y47R) control mice [17–20]. C57BL/6 mice were also used as background controls. Including background and transgene controls, 40 age– (16 ± 0.18 months, 10 per group, 5 males and

**Table 1**
Assessment of stability of expression of housekeeping genes in PSC-derived RPE cells.

| Targets | RPE 1 | RPE 2 | RPE 3 |
|---------|-------|-------|-------|
| 18s | 13.96 | 13.98 | 11.96 |
| GAPDH | 20.98 | 21.97 | 20.99 |
| HPRT1 | 28.96 | 28.95 | 27.95 |
| GUSB | 27.98 | 27.96 | 27.97 |
| **ACTB** | **21.98** | **21.98** | **21.00** |
| B2M | 23.95 | 23.95 | 22.95 |
| RPLP0 | 23.95 | 23.95 | 22.94 |
| HMBS | 29.94 | 29.94 | 29.95 |
| TBP | 30.94 | 29.94 | 29.95 |
| PGK1 | 23.93 | 24.93 | 22.94 |
| UBC | 23.95 | 24.94 | 23.94 |
| PPIA | 22.96 | 23.96 | 22.96 |

qRT-PCR were performed using three different PSC-derived RPE cells from three independent experiments. Data are shown as raw Ct values. ACTB (bold) was chosen as the reference housekeeping gene.

5 females) and sex- matched mouse eyes were immersion-fixed in 4% PFA and processed to paraffin.

### 2.3. Morphometric analysis of mouse retinal sections

Sagittal sections were stained with haematoxylin and eosin (H&E) and the thicknesses of various retinal layers and RPE were measured using Image J (Image J v1.46r, NIH, USA). Cell counts were also performed on the RGC layer. All analysis was performed blinded to the identity of the sections. Four measurements from four equivalent regions across each retina were obtained in triplicate serial sections for each animal. For analysis, measurements were normalized to the thickness of the entire retina (INL-ONL) except for the inner retina layers which were normalized across the inner retina, to account for obliquely cut sections.

### 2.4. Collection of human eyes

Six human eyes from individuals with FRDA were collected during autopsy, together with other tissues, and were de-identified before delivery to the researchers. Briefly, eyes were removed either through enucleation or through the orbital roof after removal of the brain. They were then fixed by immersion in formalin. After 1 h, a frontal cut was performed through the eyes to allow formalin to reach the retina.

### 2.5. Pathology of post-mortem FRDA eyes

The six fixed post-mortem eyes from FRDA patients were hand processed through graded alcohols and xylene to paraffin. Sagittal sections were cut at 7 μm and stained with H&E. transversely sectioned at 5 μm and stained with haematoxylin and eosin and Luxol fat blue. The sixth eye had no retrobulbar optic nerve, so optic atrophy was assessed from the intrabulbar portion. All sections were assessed for abnormalities in RPE, retina, optic disc and nerve by a pathologist.

### 2.6. Cell culture

The FRDA iPSC lines FA3 and FA4 [15] and the hESC line H9 [22] were maintained as described in [15]. PSCs were differentiated into RPE cells according to [23]. After 30–60 days, pigmented cells were manually isolated and transferred to organ culture dishes in 15% fetal bovine serum (FBS) medium containing taurine, hydrocortisone and triiodothyronine (15% RPE medium) [23]. After 24 h the medium was replaced with RPE medium containing 5% FBS
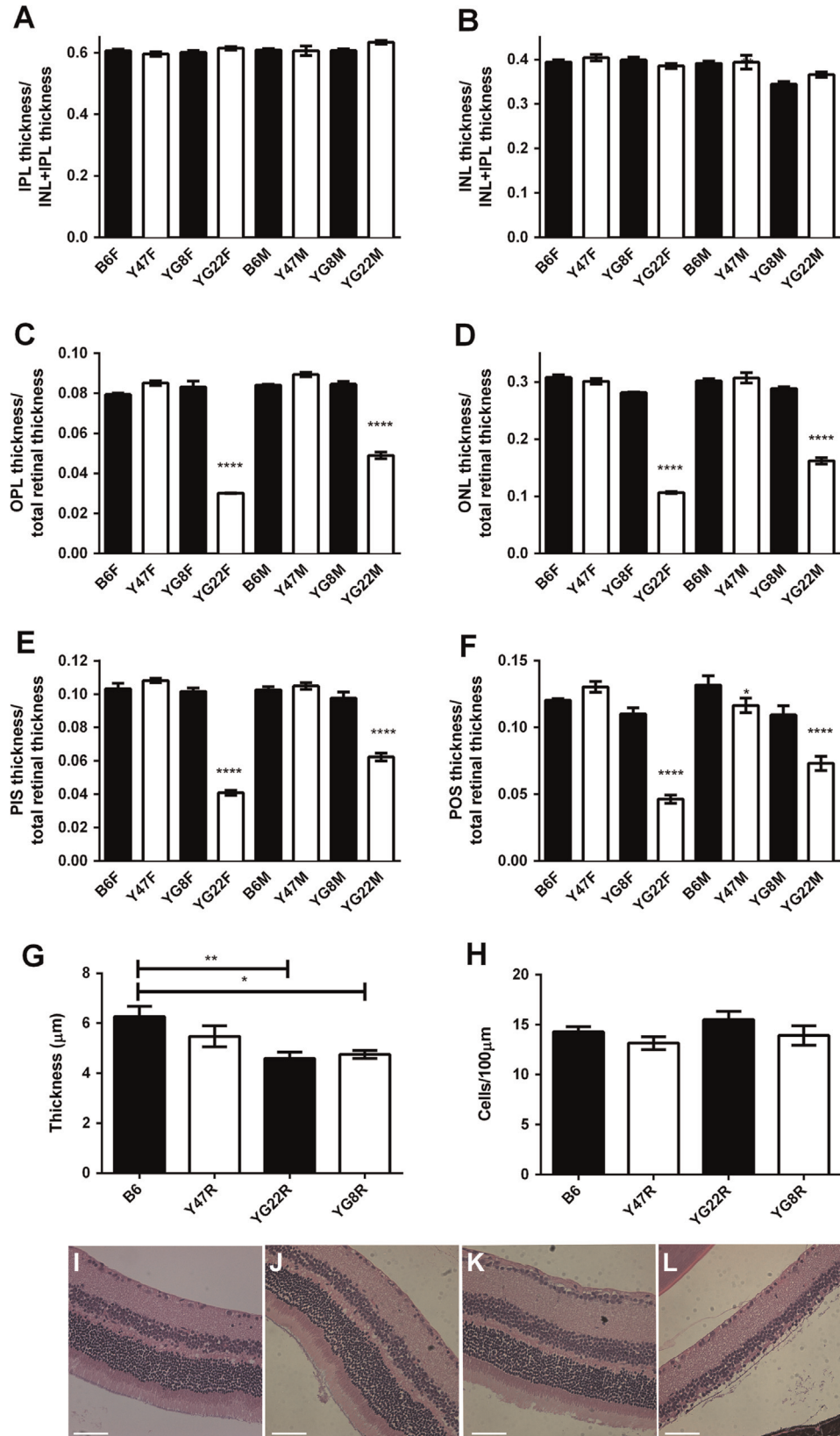
**Fig. 1.** Histomorphometric analysis of mouse retinas. Measurement in female (F) and male (M) mice of the IPL (A), INL (B), OPL (**C**), ONL (D), PIS/POS (E–F) in C57BL/6 (B6), Y47R, YG8R and YG22R mice. Analysis of RPE (G) and RGC count (H) demonstrated no significant differences between sex so these data were combined for assessment. Data is expressed as mean $\pm$ SEM relative thickness (A–F), thickness (G) or cell number (H). (A–H) Statistics 2-way ANOVA with Bonferroni's multiple comparison test. $^{*}p < 0.05$ $^{**}p < 0.01$, $^{****}p < 0.0001$. $n = 10$ mice per group (5 males, 5 females); 4 measurements from 4 equivalent regions across each retina were obtained in triplicate serial sections for each animal. (I–L) Representative images of sections used for analysis in C57BL/6 (I), Y47R (J), YG8R (K) and YG22R (L) mice. Scale bar: 50 $\mu$m.
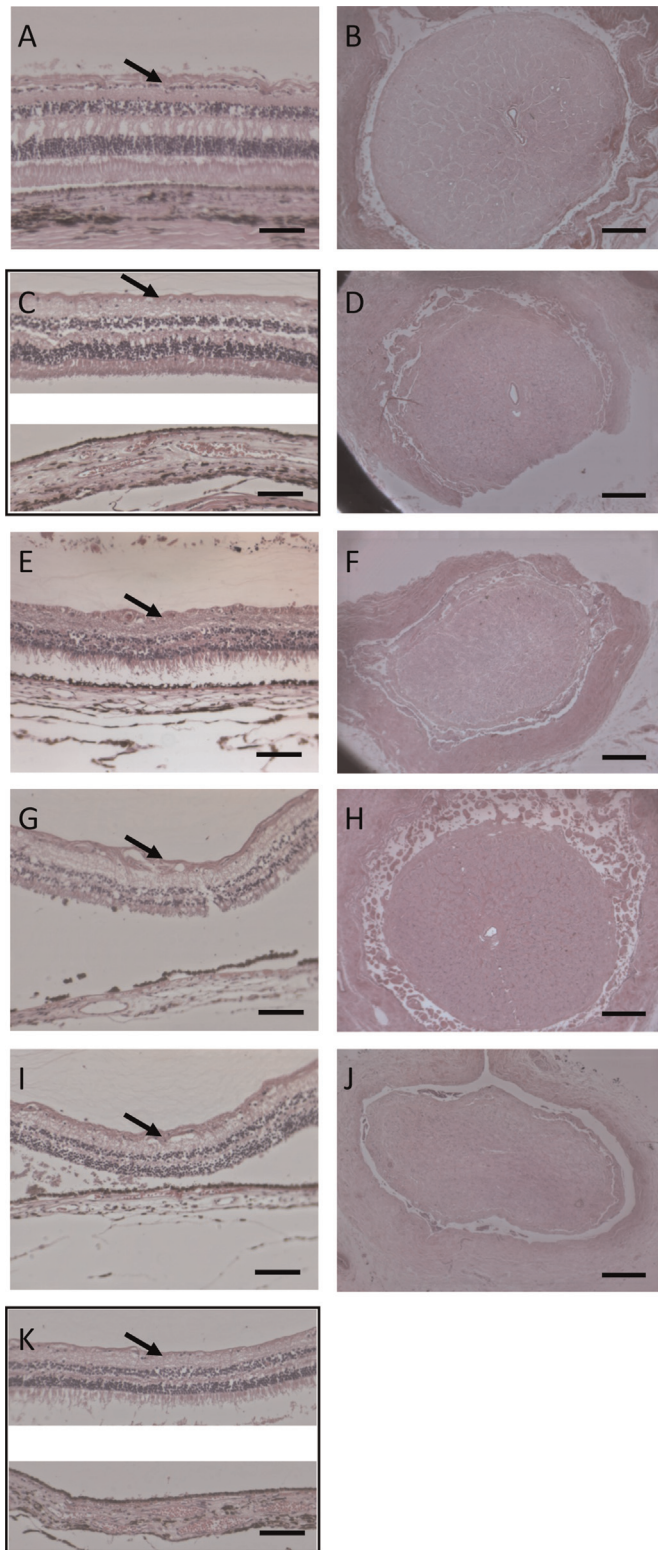
**Fig. 2.** Histochemistry staining of FRDA human eyes. H&E stained retinal (left column, ×20 objective) and optic nerve sections (right column, ×4 objective) from FRDA post-mortem tissues from sample 1 (A, B) a FRDA patient with normal optic nerve and retina; 2 (C, D), 3 (E, F), 4 (G, H), 5 (I, J) and 6 (K), demonstrating varying degrees of optic nerve atrophy and cell loss from the RGC layer (arrows). Extra-bulbar optic nerve from sample 6 was not available for analysis. Scale bars: 100 μm for retinal sections, 500 μm for optic nerve sections.

(5% RPE medium) [23]. Confluent RPE cells were subsequently passaged up to three times with 0.25% Trypsin–EDTA at a density of 50,000–100,000 cells per cm$^2$ in 15% RPE medium. Once

attached, RPE cells were switched to 5% RPE medium and expanded until confluence, re-pigmentation and mature polygonal morphology were observed. RPE cells were used for assays between passage 1–3 post manual isolation.

### 2.7. qPCR for markers of RPE cells and FXN expression

RNA extraction and cDNA synthesis was performed using the RNeasy Minikit (Qiagen) and the High-Capacity cDNA reverse transcription kit (Invitrogen) as per manufacturers instruction. qPCR was performed on a 7900HT Fast Realtime PCR system (Applied Biosystems) with 2ng of cDNA per reaction, using the following primers: GAPDH (Hs 99999905_m1), HPRT1 (Hs99999909_m1), GUSB (Hs99999908_m1), beta-ACTIN (ACTB, Hs99999903_m1), B2M (Hs99999907_m1), RPLP0 (Hs99999902_m1), HMBS (Hs00609297_m1), TBP (Hs99999910_m1), PGK1 (Hs99999906_m1), UBC (Hs00824723_m1), PPIA (Hs99999904_m1), PAX6 (Hs00240871_m1), SIX3 (Hs00193667_m1), RAX (Hs00429459_m1), MITF (Hs01117294_m1), PMEL (Hs00173854_m1), RLBP1 (Hs00165632_m1), RPE65 (Hs01071462_m1) and FXN (Hs00175940_m1). Housekeeping genes were assessed for their stability of expression in three independent cultures of PSC-derived RPE cells (Table 1). Subsequently, ACTB was selected as the housekeeping gene. Data is expressed as mean ± SEM relative gene expression using the delta-delta CT method for each gene assay measured.

### 2.8. High resolution respirometry

Maximal mitochondrial respiration was measured by providing artificially high levels of complex-I and –II substrates in the presence of excess ADP to maximize coupled mitochondrial respiration rates, as described in [24]. Mitochondrial respiration was uncoupled from the inhibitory feedback loop on OXPHOS provided by ATP synthase with addition of the uncoupler carbonyl cyanide m-chlorophenyl hydrazone (CCCP). Residual oxygen consumption was measured by adding rotenone and antimycin A. Briefly, 24 h prior to experiment, RPE medium was changed. $1.5 \times 10^6$ RPE cells harvested by trypsinisation for 10 min were re-suspended in respiration buffer (200 mM sucrose, 20 mM taurine, 20 mM HEPES, 10 mM KH$_2$PO$_4$, 3 mM MgCl$_2$, 3 mM EGTA, 1 g/L fatty acid free BSA; pH 7.1) as described [25] and added to each chamber. Following equilibration with ambient oxygen for at least 10 min with stirring, the chamber was closed. Glutamate (10 mM) and malate (2 mM) were added, followed by the optimized digitonin concentration (10 μg/mL) for each cell line. ADP (1 mM), succinate (10 mM), CCCP (1.5 μM), rotenone (5 μM) and antimycin A (2 μM) were added at intervals of approximately 2 min. Respiration states measured included endogenous respiration rate (with endogenous substrates), ADP-stimulated cell respiration with glutamate+malate (CxI-ADP) or with succinate (CxI+II-ADP) and the uncoupled maximal respiration (UC) by the addition of CCCP. On average the residual oxygen consumption (ROX; when rotenone and antimycin A inhibited mitochondrial respiration) was less than 1% of the UC rate.

### 2.9. Photoreceptor outer segments (POS) isolation and labeling

POS were isolated according to established protocols [26,27] from 40 bovine eyes fresh from the slaughterhouse. POS were incubated with 0.4 mg/mL Fluorescein isothyocyanate (FITC) isomer (Life Technologies) for 1.5 h at room temperature with gentle rotation. FITC-labeled POS (FITC-POS) were washed twice in 10% sucrose, 20 mM sodium phosphate pH 7.2, 5 mM taurine, then once in DMEM, and resuspended in DMEM with 2.5% sucrose, counted, aliquoted and stored at −80 C.

**Table 2**
FRDA post-mortem eye pathology

| Sample | Gender | Age of onset (y) | Age of death (y) | Disease duration (y) | GAA repeats | Cause of death (heart weight) | Pathology |
|--------|--------|------------------|------------------|----------------------|-------------|-------------------------------|-----------|
| 1 | M | 10 | 24 | 14 | 1050/700 | Cardiomyopathy (565) | Mild concavity of the optic disc - some artefactual processing issues - essentially normal optic nerve and retina |
| 2 | F | 15 | 69 | 54 | 560/560 | Cardiomyopathy (359) | Some retinal ganglion cell loss and optic nerve atrophy - previous extracapsular cataract extraction and IOL, partial angle closure |
| 3 | M | 4 | 37 | 33 | 850/850 | Cachexia (419) | Severe retinal ganglion cell loss and optic nerve atrophy |
| 4 | M | 9 | 33 | 24 | 925/925 | Cardiomyopathy (421) | Mild to moderate retinal ganglion cell loss |
| 5 | F | 7 | 28 | 21 | 681/837 | Cachexia (362) | Retinal ganglion cell loss and optic nerve atrophy |
| 6 | F | 5 | 25 | 20 | 734/734 | Cardiomyopathy (325) | Moderate to severe retinal ganglion cell loss and optic nerve atrophy |

### 2.10. Phagocytosis activity

Phagocytosis was assessed by flow cytometry [28]. Freshly thawed FITC-POS were diluted into $CO_2$-independent medium (Life Technologies) and incubated with RPE cells (375,000 FITC-POS per $cm^2$) for 4 h at 37 °C. Cells were harvested with 0.25% Trypsin–EDTA, incubated with 5 μM DRAQ5 as a viability dye in RPE medium, passed through a 0.45 μm cell strainer, then analyzed on a Becton Dickinson FACS Aria III flow cytometer. Data analysis was performed using FCS Express 5 (DeNovo Software). The percentage of RPE cells that internalized FITC-POS was measured from the DRAQ5-positive live cell population.

### 2.11. Statistical analysis

All statistical analyses and graphical data were generated using Graphpad Prism software (v6.02, www.graphpad.com). Statistical methods utilized were one-way and two-way ANOVA followed Bonferroni's multiple comparisons test. Data are presented as mean $\pm$ SEM. Statistical significance was established as $p < 0.05$, **$p < 0.01$, ***$p < 0.001$, ****$p < 0.0001$.

## 3. Results

### 3.1. FRDA-mouse retina analysis

Measurements of the inner plexiform layer (IPL), inner nuclear layer (INL), outer plexiform layer (OPL), outer nuclear layer (ONL), photoreceptor inner/outer segments (PIS/POS) and RPE layer thickness, as well as cell count of the RGCs on retinal sections from FRDA mutant mice and control mice were performed (Fig. 1). No significant difference in the IPL or INL was observed between the groups of mice (Fig. 1(A–B)) when corrected to the total IPL+INL thickness. A trend in reductions of the INL and POS was observed in the YG8R males but this was not statistically significant (Fig. 1(A–F)). Both male and female YG22R mice displayed a significant loss of the OPL and ONL (Fig. 1(C–D)) and a significant reduction in length of PIS and POS (Fig. 1(E–F)). Analysis of the RPE layer demonstrated no significant differences between males and females or region so these data were combined for assessment (Fig. 1(G–H)). Compared to the C57BL/6 background controls, YG8R and YG22R showed a significant thinning of the RPE layer but the thickness was not statistically different to the one measured in the Y47R transgene control mice (Fig. 1(G)). Lastly, cell count did not reveal significant modifications in RGC layer numbers in any group.

### 3.2. FRDA-post mortem eye pathology

Because of the supportive role of the RPE to photoreceptors, and given the retinal degeneration of the ONL and OPL in the mouse, we assessed the RPE layers in Humans. Also, because we did not observe variation in cell numbers of the RGC layer in the YG22R mice compared to control mice, we examined the optic nerve in Humans. Histological assessment of the six FRDA-post mortem eyes revealed variable degrees of loss of RGCs, thinning of the retinal nerve fiber layer and optic nerve atrophy (Fig. 2). The severity of optic nerve atrophy and RGC loss correlated with age of onset (Table 2), as has been previously reported [4]. No apparent abnormalities in the RPE were noted in the post-mortem eyes.

### 3.3. FRDA-iPSC-derived RPE cell analysis

To further assess a potential FRDA phenotype in the human RPE, we derived RPE cells from the FRDA-iPSCs FA3 and FA4. These cells show pigmentation and the typical cobblestone morphology, express markers of RPE cells and reduced levels of *FXN* (Fig. 3(A–C)). RPE cells were analyzed for their OXPHOS activity, in an Oxygraph 2 K high resolution respirometer with a protocol optimized for analyzing activity of Complex I and Complex II. We observed no statistical difference in FA3- and FA4-RPE cells when compared to control RPE cells (Fig. 3(D and E)). Flow cytometry analysis of phagocytosis by the FRDA-RPE cells showed that greater than 95% of FA3- and FA4-derived RPE cells were capable of phagocytosis (Fig. 3(F–H)). Altogether, this data demonstrates that despite low level of *FXN*, these cells remain functional.

## 4. Discussion

Our study demonstrated elements of outer retina degeneration with photoreceptor loss in the YG22R mouse model of FRDA. We also observed a significant thinning of the RPE layer in YG8R and YG22R when compared with the background control mice, but this was not observed when compared to the Y47R transgene control mice. This suggests an effect of transgene insertion rather than FXN deficiency. We did not observe variation in cell numbers in the ganglion cell layer, in both YG8R and YG22R. The cell count performed within this layer of the retina also accounts for displaced amacrine cells [29]. Although a variation in the balance of cell types is possible, it is unlikely, given that others showed that most neuronal changes in the aging retina is of RGCs and not interneurons such as the amacrine cells [30]. Thus our data suggest no RGC death in the two mouse models of FRDA. We did not measure the optic nerve thickness in these animals because of technical limitations in the harvesting of the mouse eyes. Yet, optic nerve degeneration can precede RGC soma loss [31,32] and we cannot exclude this possibility in these animals.

Fxn is expressed in the retina of normal mice, especially in the photoreceptors and also in the RGCs [33]. Efimova and Trottier described that in R7E mice that present with retinal degeneration, the fxn expression pattern is modified and increases as
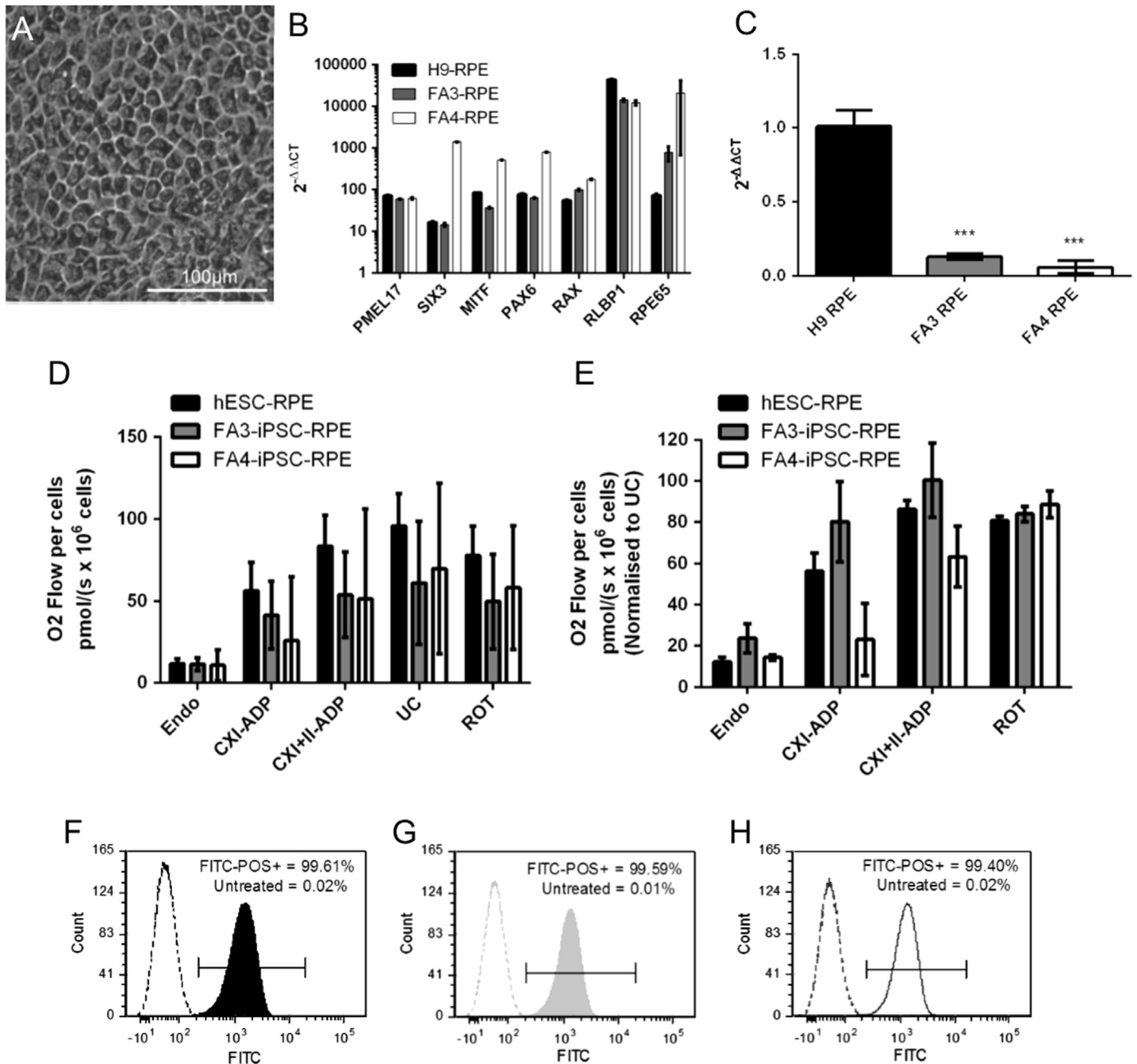
**Fig. 3.** Analysis of iPSC-derived RPE cells. (A) FRDA-iPSC-derived-RPE showing typical cobblestone morphology and pigmentation. (B) mRNA expression of RPE markers *PMEL17*, *SIX3*, *MITF*, *PAX6*, *RAX*, *RLBP1* and *RPE65* in H9-derived- (control), FA3-derived- and FA4-derived- RPE cells relative to undifferentiated cells; (C) *FXN* mRNA expression relative to H9-derived RPE cells. Data expressed as mean $\pm$ SEM relative gene expression using the delta-delta CT method for each gene assay measured. (D, E) High resolution respirometry. Respiration is shown as mean oxygen flow per million cells of endogenous unstimulated respiration (Endo), ADP stimulated complex I activity (CXI-ADP), ADP stimulated complex I+II activity (CXI+II-ADP), Maximal uncoupled respiration (UC), Maximal uncoupled respiration following complex I inhibition with Rotenone (ROT). The data normalized to UC is displayed as percentage of the UC rate. (B–E) Statistics were performed using 1-way ANOVA (B), 2-way ANOVA with Bonferroni's multiple comparison test (C, D, E), $n \geq 3$ independent experiments. ***$p < 0.001$. (F–H) Flow cytometry analysis of phagocytosis by control- (F), FA3- (G) and FA4- (H) RPE cells showing phagocytosis after incubation with FITC-POS (37 °C); controls: untreated cells.

degeneration progresses [33]. They hypothesize that this increase in fxn expression might be used by photoreceptors as a protection mechanism against apoptosis, through the anti-oxidant role of fxn [33]. In this present study, we do not know the exact amount of human FXN expressed in the mouse retina. However, we can assume that human FXN levels are lower in the retina of the YG22R and YG8R compared to the control Y47R, as the levels of FXN in the brain were found to be lower in YG22R and YG8R mice compared to Y47R [21]. Although the retinal degeneration observed in YG22R is likely to be an effect of transgene insertion rather than FXN deficiency (as there was no statistical difference observed with its

control Y47R), it remains possible that the retinal degeneration observed in the YG22R mimics the phenotype observed in the R7E as the low levels of FXN do not have sufficient anti-oxidant capabilities to protect photoreceptors from death. This however, is not a feature of the human FRDA pathology.

Using human FRDA eyes, we observed that one sample was largely regarded as normal, whilst others showed optic nerve atrophy and RGC loss, in accordance with reports from the literature [34,35]. Additionally there were no obvious morphological signs of RPE pathology in the human eyes, suggesting that if affected, the changes in these cell types could be subclinical and not

critical to disease pathogenesis. To the best of our knowledge, this study is the first to present histology of post-mortem human FRDA eyes.

Further experimentation of OXPHOS in RPE cells derived from FRDA-iPSCs demonstrated no significant changes in OXPHOS activity and normal phagocytosis in the FRDA-derived RPE cells. Altogether our data suggest that the RPE layer pathology is not a significant feature in FRDA visual dysfunction.

## Grant information

## Acknowledgments

## Appendix A. Supplementary material

Supplementary data associated with this article can be found in the online version at http://dx.doi.org/10.1016/j.bbrep.2015.09.003.

## References

[1] M.V. Evans-Galea, A. Pebay, M. Dottori, L.A. Corben, S.H. Ong, P.J. Lockhart, M. B. Delatycki, Cell and gene therapy for Friedreich ataxia: progress to date, Hum. Gene Ther. 25 (2014) 684–693.

[2] V. Campuzano, L. Montermini, M.D. Molto, L. Pianese, M. Cossee, F. Cavalcanti, E. Monros, F. Rodius, F. Duclos, A. Monticelli, F. Zara, J. Canizares, H. Koutnikova, S.I. Bidichandani, C. Gellera, A. Brice, P. Trouillas, G. De Michele, A. Filla, R. De Frutos, F. Palau, P.I. Patel, S. Di Donato, J.L. Mandel, S. Cocozza, M. Koenig, M. Pandolfo, Friedreich's ataxia: autosomal recessive disease caused by an intronic GAA triplet repeat expansion, Science 271 (1996) 1423–1427.

[3] C.D. Alldredge, C.R. Schlieve, N.R. Miller, L.A. Levin, Pathophysiology of the optic neuropathy associated with Friedreich ataxia, Arch. Ophthalmol. 121 (2003) 1582–1585.

[4] F. Fortuna, P. Barboni, R. Liguori, M.L. Valentino, G. Savini, C. Gellera, C. Mariotti, G. Rizzo, C. Tonon, D. Manners, R. Lodi, A.A. Sadun, V. Carelli, Visual system involvement in patients with Friedreich's ataxia, Brain 132 (2009) 116–123.

[5] S. Noval, I. Contreras, I. Sanz-Gallego, R.K. Manrique, J. Arpa, Ophthalmic features of Friedreich ataxia, Eye 26 (2012) 315–320.

[6] L.A. Seyer, K. Galetta, J. Wilson, R. Sakai, S. Perlman, K. Mathews, G.R. Wilmot, C.M. Gomez, B. Ravina, T. Zesiewicz, K.O. Bushara, S.H. Subramony, T. Ashizawa, M.B. Delatycki, A. Brocht, L.J. Balcer, D.R. Lynch, Analysis of the visual system in Friedreich ataxia, J. Neurol. 260 (2013) 2362–2369.

[7] E. Dag, N. Ornek, K. Ornek, I.E. Erbahceci-Timur, Optical coherence tomography and visual field findings in patients with Friedreich ataxia, J. Neuroophthalmol. 34 (2014) 118–121.

[8] B. Diehl, M.S. Lee, J.R. Reid, C.D. Nielsen, M.R. Natowicz, Atypical, perhaps under-recognized? An unusual phenotype of Friedreich ataxia, Neurogenetics 11 (2010) 261–265.

[9] X. He, P. Hahn, J. Iacovelli, R. Wong, C. King, R. Bhisitkul, M. Massaro-Giordano, J.L. Dunaief, Iron homeostasis and toxicity in retinal degeneration, Prog. Retin. Eye Res. 26 (2007) 649–673.

[10] R.W. Wong, D.C. Richa, P. Hahn, W.R. Green, J.L. Dunaief, Iron toxicity as a potential factor in AMD, Retina 27 (2007) 997–1003.

[11] D. Song, J.L. Dunaief, Retinal iron homeostasis in health and disease, Front. Aging Neurosci. 5 (2013) 24.

[12] H. Chen, T.J. Lukas, N. Du, G. Suyeoka, A.H. Neufeld, Dysfunction of the retinal pigment epithelium with age: increased iron decreases phagocytosis and lysosomal activity, Invest. Ophthalmol. Vis. Sci. 50 (2009) 1895–1902.

[13] A. Hick, M. Wattenhofer-Donzé, S. Chintawar, P. Tropel, J.P. Simard, N. Vaucamps, D. Gall, L. Lambot, C. André, L. Reutenauer, M. Rai, M. Teletin, N. Messaddeq, S.N. Schiffmann, S. Viville, C.E. Pearson, M. Pandolfo, H. Puccio, Neurons and cardiomyocytes derived from induced pluripotent stem cells as a model for mitochondrial defects in Friedreich's ataxia, Dis. Models Mech. 6 (2013) 608–621.

[14] S. Ku, E. Soragni, E. Campau, E.A. Thomas, G. Altun, L.C. Laurent, J.F. Loring, M. Napierala, J.M. Gottesfeld, Friedreich's ataxia induced pluripotent stem cells model intergenerational GAATTC triplet repeat instability, Cell Stem Cell 7 (2010) 631–637.

[15] J. Liu, P.J. Verma, M.V. Evans-Galea, M.B. Delatycki, A. Michalska, J. Leung, D. Crombie, J.P. Sarsero, R. Williamson, A. Dottori, A. Pebay, Generation of induced pluripotent stem cell lines from Friedreich ataxia patients, Stem Cell Rev. 7 (2011) 703–713.

[16] Y.K. Lee, P.W. Ho, R. Schick, Y.M. Lau, W.H. Lai, T. Zhou, Y. Li, K.M. Ng, S.L. Ho, M. A. Esteban, O. Binah, H.F. Tse, C.W. Siu, Modeling of Friedreich ataxia-related iron overloading cardiomyopathy using patient-specific-induced pluripotent stem cells, Pflugers Arch. 466 (2014) 1831–1844.

[17] M.A. Pook, S. Al-Mahdawi, C.J. Carroll, M. Cossee, H. Puccio, L. Lawrence, P. Clark, M.B. Lowrie, J.L. Bradley, J.M. Cooper, M. Koenig, S. Chamberlain, Rescue of the Friedreich's ataxia knockout mouse by human YAC transgenesis, Neurogenetics 3 (2001) 185–193.

[18] S. Al-Mahdawi, R.M. Pinto, D. Varshney, L. Lawrence, M.B. Lowrie, S. Hughes, Z. Webster, J. Blake, J.M. Cooper, R. King, M.A. Pook, GAA repeat expansion mutation mouse models of Friedreich ataxia exhibit oxidative stress leading to progressive neuronal and cardiac pathology, Genomics 88 (2006) 580–590.

[19] S. Al-Mahdawi, R.M. Pinto, P. Ruddle, C. Carroll, Z. Webster, M. Pook, GAA repeat instability in Friedreich ataxia YAC transgenic mice, Genomics 84 (2004) 301–310.

[20] S. Al-Mahdawi, R.M. Pinto, O. Ismail, D. Varshney, S. Lymperi, C. Sandi, D. Trabzuni, M. Pook, The Friedreich ataxia GAA repeat expansion mutation induces comparable epigenetic changes in human and transgenic mouse brain and heart tissues, Hum. Mol. Genet. 17 (2008) 735–746.

[21] S. Anjomani Virmouni, C. Sandi, S. Al-Mahdawi, M.A. Pook, Cellular, molecular and functional characterisation of yac transgenic mouse models of friedreich ataxia, PLoS One 9 (2014) e107416.

[22] J.A. Thomson, J. Itskovitz-Eldor, S.S. Shapiro, M.A. Waknitz, J.J. Swiergiel, V. S. Marshall, J.M. Jones, Embryonic stem cell lines derived from human blastocysts, Science 282 (1998) 1145–1147.

[23] A. Maminishkis, S. Chen, S. Jalickee, T. Banzon, G. Shi, F.E. Wang, T. Ehalt, J. A. Hammer, S.S. Miller, Confluent monolayers of cultured human fetal retinal pigment epithelium exhibit morphology and physiology of native tissue, Invest. Ophthalmol. Vis. Sci. 47 (2006) 3612–3624.

[24] N.J. Van Bergen, R.E. Blake, J.G. Crowston, I.A. Trounce, Oxidative phosphorylation measurement in cell lines and tissues, Mitochondrion 15 (2014) 24–33.

[25] S. Stadlmann, G. Rieger, A. Amberger, A.V. Kuznetsov, R. Margreiter, E. Gnaiger, $H_2O_2$-mediated oxidative stress versus cold ischemia-reperfusion: mitochondrial respiratory defects in cultured human endothelial cells, Transplantation 74 (2002) 1800–1803.

[26] R.S. Molday, D. Hicks, L. Molday, Peripherin. A rim-specific membrane protein of rod outer segment discs, Invest. Ophthalmol. Vis. Sci. 28 (1987) 50–61.

[27] R. Singh, M.J. Phillips, D. Kuai, J. Meyer, J.M. Martin, M.A. Smith, E.T. Perez, W. Shen, K.A. Wallace, E.E. Capowski, L.S. Wright, D.M. Gamm, Functional analysis of serially expanded human iPS cell-derived RPE cultures, Invest. Ophthalmol. Vis. Sci. 54 (2013) 6767–6778.

[28] P.D. Westenskow, S.K. Moreno, T.U. Krohne, T. Kurihara, S. Zhu, Z.N. Zhang, T. Zhao, Y. Xu, S. Ding, M. Friedlander, Using flow cytometry to compare the dynamics of photoreceptor outer segment phagocytosis in iPS-derived RPE cells, Invest. Ophthalmol. Vis. Sci. 53 (2012) 6282–6290.

[29] C.J. Jeon, E. Strettoi, R.H. Masland, The major cell populations of the mouse retina, J. Neurosci. 18 (1998) 8936–8946.

[30] M.A. Samuel, Y. Zhang, M. Meister, J.R. Sanes, Age-related alterations in neurons of the mouse retina, J. Neurosci. 31 (2011) 16033–16044.

[31] B.P. Buckingham, D.M. Inman, W. Lambert, E. Oglesby, D.J. Calkins, M.R. Steele, M.L. Vetter, N. Marsh-Armstrong, P.J. Horner, Progressive ganglion cell degeneration precedes neuronal loss in a mouse model of glaucoma, J. Neurosci. 28 (2008) 2735–2744.

[32] D.J. Calkins, Age-related changes in the visual pathways: blame it on the axon, Invest. Ophthalmol. Vis. Sci. 54 (2013) 41, ORSF37.

[33] M.G. Efimova, Y. Trottier, Distribution of frataxin in eye retina of normal mice and of transgenic R7E mice with retinal degeneration, J. Evolut. Biochem. Physiol. 46 (2010) 414–417.

[34] M.H. Parkinson, S. Boesch, W. Nachbauer, C. Mariotti, P. Giunti, Clinical features of Friedreich's ataxia: classical and atypical phenotypes, J. Neurochem. 126 (Suppl 1) (2013) S103–S117.

[35] V. Carelli, C. La Morgia, M.L. Valentino, P. Barboni, F.N. Ross-Cisneros, A. A. Sadun, Retinal ganglion cell neurodegeneration in mitochondrial inherited disorders, Biochim. Biophys. Acta 2009 (1787) 518–528.